

## Viscous Withdrawal of Miscible Liquid Layers

Laura E. Schmidt and Wendy W. Zhang

*The Department of Physics & The James Franck Institute, University of Chicago, Chicago, Illinois 60637, USA*  
(Received 31 August 2007; published 28 January 2008)

In viscous withdrawal, a converging flow imposed in an upper layer of viscous liquid entrains liquid from a lower, stably stratified layer. Using the idea that a thin tendril is entrained by a local straining flow, we propose a scaling law for the volume flux of liquid entrained from miscible liquid layers. A long-wavelength model including only local information about the withdrawal flow is degenerate, with multiple tendril solutions for one withdrawal condition. Including information about the global geometry of the withdrawal flow removes the degeneracy while introducing only a logarithmic dependence on the global flow parameters into the scaling law.

DOI: [10.1103/PhysRevLett.100.044502](https://doi.org/10.1103/PhysRevLett.100.044502)

PACS numbers: 47.55.N-, 68.05.-n, 47.15.Rq

Recent experiments on thermal convection with two layers of miscible liquids reveal several distinct regimes—an overturn regime with violent mixing of the layers, a doming regime where the interface undulates, and a stratified regime where the convection is largely stable with thin tendrils or sheets of one liquid entrained within the other [1]. Similar steady-state entrained structures arise in drainage flows [2,3], oil extraction [4], as well as viscous withdrawal of immiscible liquid layers, which occur in microfluidics [5], fiber coating [6], and encapsulation of biological cells [7]. Whether the entrained structure in fact becomes isolated from the large-scale flow dynamics at the onset of entrainment remains an open question [2,8–10]. One signal of this decoupling is the evolution of the tendril base shape towards a power-law cusp. Intriguingly, experiments [11,12] on miscible entrainment seem to show a robust cusplike shape at the base of long-lived tendrils (see Fig. 1). This suggests the entrained tendrils are isolated from the fluctuating, large-scale convection by the cusp-shaped base and are therefore able to remain stable over many convection cycles. If true, this may explain why hot spots can persist over many convection cycles in the Earth’s mantle [12,13]. Motivated by these observations, we focus on the stratified regime in thermal convection of miscible layers and present a model that tests how a thin cylindrical tendril is anchored in the large-scale flow.

Because the large-scale flow is stabilized in the stratified regime, mixing between the layers is controlled by the volume flux of liquid entrained through the tendrils,  $Q_0$ . Existing estimates of  $Q_0$  assume that the velocity field inside the tendril is uniformly upwards, flowing at a characteristic convection speed [11,12,14]. However, recent particle-image-velocimetry (PIV) measurements reveal the interior flow can have a more complex structure (Fig. 2): a thin layer of the lower-layer liquid directly beneath the interface moves inwards and is entrained downstream, but most of the lower-layer liquid simply recirculates, thus creating a stagnation-point velocity field inside the tendril [15]. Analogous withdrawal experiments on immiscible liquid layers shed light on how this more

complex velocity field arises [8]. When the effect of the entrainment penetrates deeply into the lower layer, a broad tendril forms with the interior moving uniformly upwards, consistent with the scenario assumed in the existing estimates. However, when the effect of the entrainment penetrates weakly, a narrow tendril forms by drawing liquid inward within a thin layer below the interface, thus creating an interior stagnation point. This is the scenario we analyze here, first qualitatively via a scaling analysis and then quantitatively.

Since the steady-state flow fields associated with nonlinear interface deformations are difficult to obtain analytically, we start by analyzing the simplest situation in accord with the interior stagnation-flow scenario. We will examine the steady-state entrainment of a tendril from a deep lower layer by an axisymmetric viscous withdrawal flow imposed in an upper layer (Fig. 2). The entrained liquid is taken to be much less viscous than the exterior so that there is only a weak feedback from entrained flow to the withdrawal flow. To ensure that the effect of entrainment penetrates only weakly into the lower layer, we require that the layers are strongly stratified. With these simplifications, the steady-



FIG. 1 (color online). Axisymmetric tendrils entrained by a warmer, upwards flow in a 2-layer thermal convection experiment with miscible oils. Convection is driven by heating the bottom of the tank and cooling the top. The lower fluid is less viscous than the upper, and the spacing between tendrils is  $O(10\text{ cm})$ . The dark vertical line on the left is a thermocouple [13].

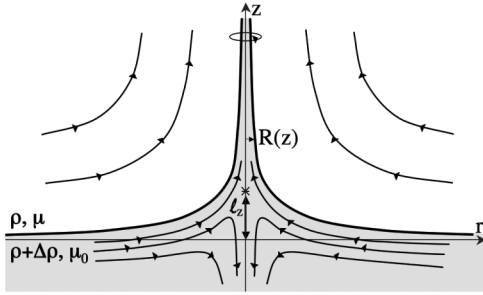


FIG. 2. Sketch of surface  $R(z)$  and flow streamlines for an axisymmetric withdrawal flow in the upper liquid layer entraining a thin, cylindrical tendril from a deep lower layer.

state interface divides into three geometrically distinct regions: a long and slender entrained tendril where interior flow effects are dominant, a far-field interface where the hydrostatic pressure is dominant, and a transition region. We use a cylindrical coordinate system where  $z = 0$  corresponds to the height of the undisturbed interface, and  $r = 0$  corresponds to the center line of the tendril. The tendril radius is  $R(z)$ .

We start by estimating the key features of the large-scale withdrawal dynamics. To keep the scaling analysis simple, we assume that the geometry of the large-scale withdrawal flow in the upper layer is irrelevant, and approximate it by an axisymmetric straining flow,  $(-Er/2)\mathbf{e}_r + Ez\mathbf{e}_z$  where  $E$  ( $s^{-1}$ ) is the rate of strain, consistent with the existence of a stagnation point. (We will see later in the full analysis that, while this simplification is acceptable for the scaling analysis, it is also incomplete.) Balancing the upwards pull exerted by the viscous stresses in the withdrawal flow against the hydrostatic pressure defines a characteristic vertical length scale

$$\ell_z = 2\mu E / \Delta\rho g. \quad (1)$$

If no liquid is entrained from the lower layer, the length scale  $\ell_z$  is simply the deflection height of the unbroken interface. When a thin tendril of liquid is entrained, the length scale  $\ell_z$  is the upward deflection of the recirculation cell in the lower layer.

In steady-state, the small-scale entrained flow within the tendril must be consistent with the large-scale dynamics. To examine the small-scale flow, we use the assumption that the tendril is long and slender so that the interior velocity field can be approximated via standard slender-body type arguments [16]. There are three distinct components in the interior flow field. First, an upwards-moving plug flow  $u_+(z) = Ez$  induced by the upwards moving flow in the exterior. Second, a Poiseuille flow  $u_p(r, z) = -(dP_0/dz)[R^2(z) - r^2]/(4\mu_0)$  component driven by the interior pressure gradient  $dP_0/dz$ . To estimate  $P_0$ , note that the exterior withdrawal flow has a form that speeds up and draws liquid radially inwards as one moves downstream. This exerts an  $O(\mu E)$  inward squeeze on the surface, one which is balanced by an  $O(\mu E)$  interior pressure. Finally, there is a drainage flow  $u_-(r, z) =$

$-(\Delta\rho g)[R^2(z) - r^2]/(4\mu_0)$  due to the hydrostatic pressure. Balancing  $u_+$  and  $u_p$  at the interior stagnation point on the center line, which has height  $O(\ell_z)$ , yields a characteristic tendril radius size

$$\ell_R = \sqrt{\frac{4\mu_0 E \ell_z}{\Delta\rho g}} = \sqrt{2\left(\frac{2\mu_0 E}{\Delta\rho g}\right)\left(\frac{2\mu E}{\Delta\rho g}\right)}. \quad (2)$$

This also shows that the drainage flow  $u_-$ , of roughly size  $\Delta\rho g \ell_R^2 / (4\mu_0)$  at the stagnation point, is comparable in size with both  $u_+$  and  $u_p$ . The expression for  $\ell_R$  confirms that the tendril ‘‘slenderness ratio,’’  $\ell_R/\ell_z$ , assumed to be small at the beginning of our analysis, is  $\sqrt{2\mu_0/\mu}$ , which is indeed small for  $\mu_0 \ll \mu$ .

Given  $\ell_z$  and  $\ell_R$ , we can rewrite  $Q_0$ , the volume flux of the liquid entrained from the lower layer, as

$$Q_0 = c_0(E\ell_z)(\pi\ell_R^2) = c_0(16\pi\mu^2\mu_0 E^4)/(\Delta\rho g)^3, \quad (3)$$

where  $c_0$  is a dimensionless entrainment coefficient. If our starting assumption that the global geometry has no effect on the entrainment dynamics is correct, then  $c_0$  would be a universal constant, independent of the precise detail of the convection in the upper layer. We will show in the full analysis that, in fact, some weak dependence on the global geometry is present, resulting in logarithmic variations in the value of  $c_0$  with the global geometry. The important point is that the scaling analysis captures the main features of the entrainment dynamics. The scaling law (3) differs from existing estimates based on a characteristic convection velocity  $U$  [11,12,14]. If we take  $S$  as the size of the convection cell, then (3) gives  $Q_0 \propto (U/S)^4$  while existing estimates give  $Q_0 \propto U^3$ . Interestingly, nothing in the above scaling argument depends in an apparent way on the withdrawal being axisymmetric. An analogous argument for entrained 2-D sheets yields the same relations for  $\ell_z$  (1) and the sheet thickness  $\ell_R$  (2), and the scaling law  $Q_0/L \approx E\ell_z\ell_R$  for the volume flux per unit length.

We next develop a long-wavelength model of the entrainment dynamics and find that a model which includes only the local straining flow is degenerate. For each value of  $Q_0$ , there exists a continuous family of tendril solutions, each with a different power-law shape at the base. Including the large-scale withdrawal flow geometry removes this degeneracy. Physically, this is because the tendril size at its base, where the tendril joins onto the interface, is controlled by how the interfaces levels out on the large length scale. This leveling out is sensitive to the global geometry of the withdrawal flow. As a result, the entrainment dynamics, and specifically the entrainment flux  $Q_0$ , have a logarithmic dependence on the global dynamics. The logarithmic dependence on the global geometry effectively shields the tendril from fluctuations in the upper layer flow which occur far from the tendril.

Starting with the Navier-Stokes equations, and using standard slender-body approximations where effects proportional to  $\ell_R/\ell_z$  are discarded at leading-order, we derive the following equation for the steady-state tendril shape

$$Q_0 = (Ez)\pi R^2(z) - \frac{\pi R^4(z)}{8\mu_0} \left( \frac{dP_0}{dz} + \Delta\rho g \right). \quad (4)$$

In essence, Eq. (4) says that the *unknown* volume flux of liquid entrained into the tendril has three contributions: a plug flow  $Ez$  induced by the withdrawal, pipe flows associated with the nonuniform interior pressure,  $P_0$ , and the hydrostatic pressure difference. An expression for  $P_0$  is derived from the normal stress balance across the surface of the tendril:

$$P_0 = 2\mu E \left( 1 + \frac{z}{R(z)} \frac{dR}{dz} \right). \quad (5)$$

This represents the large pressure necessary to keep a tendril from collapsing under the inward squeeze exerted by the exterior straining flow. Equations (4) and (5) together yield a second-order nonlinear ordinary differential equation for the steady-state tendril shape  $R(z)$  and  $Q_0$ . The derivation is analogous to the entrainment model for immiscible liquids in [10], except that the surface tension contribution to  $P_0$  is replaced here by the hydrostatic pressure difference.

The natural boundary conditions are conditions on how the tendril shape  $R(z)$  tapers to 0 downstream as  $z \rightarrow \infty$  and how  $R(z)$  flares out into a flat interface upstream as  $z \rightarrow 0$ . Both conditions correspond to asymptotic balances of the governing equations. Far above the interface, the asymptotic balance indicates that  $R(z)$  tapers so strongly with  $z$  that the upwards plug flow  $Ez$  dominates over  $u_p$  and  $u_-$  so that

$$R(z) \rightarrow R_\infty(z) = \sqrt{Q_0(c_0)/(\pi Ez)} \quad \text{as } z \rightarrow \infty, \quad (6)$$

where we have written  $Q_0(c_0)$  to emphasize that in our analysis, we use the scaling law (3) for  $Q_0$  so that  $c_0$  is the only undetermined parameter. Near the tendril base, the effects of entrainment are negligible because the layers are strongly stratified. The tendril base shape is therefore determined by a balance of the hydrostatic pressure and the exterior viscous stress; thus,

$$R(z) \rightarrow R_s(z) = B \left( \frac{\ell_z}{z} \right)^\alpha e^{-z/\ell_z} \quad \text{as } z \rightarrow 0. \quad (7)$$

Both the coefficient  $B$  and the exponent  $\alpha$  need to be determined self-consistently with the full solution.

Using boundary conditions (6) and (7), and appropriate downstream structural stability modes, we numerically integrated Eqs. (4) and (5) for tendril solutions [17]. We found that, for a fixed  $Q_0$ , a continuous family of tendril solutions exist. Each solution's upstream shape is characterized by a different set of  $\alpha$  and  $B$  values. Figure 3 gives a few examples of the different tendrils possible for the same volume flux. The long-wavelength model is therefore clearly degenerate.

Removing the degeneracy requires an additional condition on the upstream shape, one related to the large-scale topography. We next show this explicitly. In our toy model,

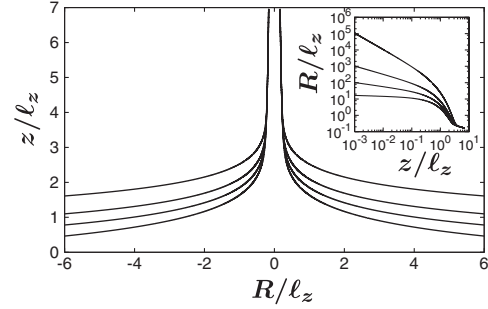


FIG. 3. Rescaled tendril solutions at  $S/\ell_z = 15$ ,  $\mu_0/\mu = 0.1$ ,  $c_0 = 3.1$  with exponents  $\alpha = 1.0, 0.5, 0.25, 0.052$  (top to bottom). Inset shows tendrils have different power-law divergences.

an axisymmetric withdrawal flow is generated in the upper layer by inserting a point force with strength  $F$  at a height  $S$  above the undisturbed interface. This is clearly not a realistic withdrawal near the point force but, if  $S$  is large, it is a good approximation of realistic withdrawal flows near the interface. The velocity fields in both fluid layers can be obtained by a variation of the method of images [18] and correspond to an axisymmetric straining flow with  $E = F/(2\pi\mu S^2)$  in the neighborhood of the base of the tendril. Since the effects of entrainment penetrate weakly into the lower layer, the large-scale interface shape is the deflection when no liquid is entrained,

$$R_I(z) = S\sqrt{(3\ell_z/2z)^{2/5} - 1}. \quad (8)$$

The fact that  $R_I(z)$  is controlled by  $S$  is the extra information needed to uniquely select a tendril solution.

To incorporate this extra information, we require that at an unknown location  $z_s$ , the tendril shape, as well as  $dR/dz$  and  $d^2R/dz^2$ , equal the corresponding quantities in  $R_I(z)$  [19]. We solve for  $z_s$ ,  $\alpha$  and  $B$  analytically as follows. Since  $z_s$  should be near the base of the tendril, we approximate  $R(z)$  by the upstream shape  $R_s$  (7) and find that  $z_s \approx 0.609\ell_z$ ,  $\alpha \approx 0.052$ , and  $B \approx 1.18S$ . We also solved for the appropriate tendril solution numerically by varying the dimensionless entrainment coefficient  $c_0$  so that  $R(z)$  and its derivative merge smoothly onto  $R_I(z)$  and found results consistent with the analytic estimates. Figure 4 shows an example of how  $c_0$  is found numerically.

It is interesting to know how the dimensionless entrainment coefficient  $c_0$  depends on the global length scale,  $S/\ell_z$ , and on the viscosity contrast  $\mu_0/\mu$ . We have varied  $S/\ell_z$  from 10 to  $10^8$  and  $\mu_0/\mu$  from  $10^{-1}$  to  $10^{-6}$  and plotted the results in the inset of Fig. 4. The variation of  $c_0$  with these parameters is unexpectedly simple, well approximated by  $c_0 \approx 2.3 \log[S/(\ell_z\sqrt{\mu_0/\mu})] - 0.74$ . The logarithmic dependencies of  $c_0$  on  $S/\ell_z$  and  $\mu_0/\mu$  are weaker than the power-law dependencies of  $Q_0$  on  $\ell_z$  and  $\mu_0/\mu$  in the scaling law (3). This shows that including the global dynamics only weakly modifies the simple entrainment law.

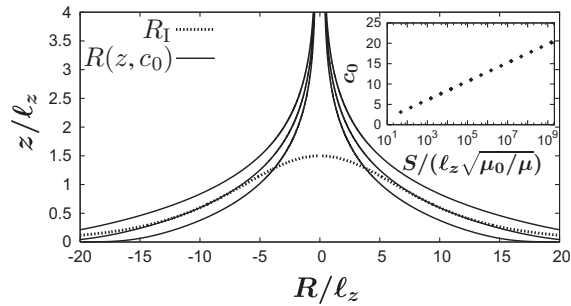


FIG. 4. Rescaled tendril solutions  $R(z)$  for  $c_0 = 3.4, 3.1,$  and  $2.9$  (solid lines, top to bottom), together with the large-scale deflection solution  $R_I(z)$  (dotted line) for  $S/\ell_z = 15$  and  $\mu_0/\mu = 0.1$ . Only  $c_0 = 3.1$  allows the two shapes to merge smoothly. Inset shows  $c_0$  increases logarithmically with  $S/(\ell_z\sqrt{\mu_0/\mu})$ .

The logarithmic dependence ultimately results from the decaying exponential shape of the tendril at  $z \sim \ell_z$  (7). How this emerges is complicated because  $c_0$  is essentially determined by demanding  $R_\infty(z)$  merge onto  $R_s(z)$  through a region where all the terms in the governing Eq. (4) are equally important. Our rough analysis shows that two requirements appear necessary for the observed  $c_0$  relation. First, the upstream tendril shape  $R_s(z)$  should assume a size consistent with  $R_\infty(z)$ , the steady-state downstream shape. Second, the tapering of the tendril must be accomplished by  $z \approx \ell_z$ , with the sharp exponential decay of the shape in  $dR_s(z)/dz$  appropriately switching over to a gentler square-root decay in  $dR_\infty(z)/dz$  [17].

In sum, we have now an improved scaling law for  $Q_0$ , one which explicitly accounts for the dependencies on the global flow parameters

$$Q_0 = \frac{16\pi\mu^2\mu_0E^4}{(\Delta\rho g)^3} \left[ \gamma_1 \log\left(\frac{S}{\ell_z\sqrt{\mu_0/\mu}}\right) + \gamma_2 \right], \quad (9)$$

where  $\gamma_1 \approx 2.3$  and  $\gamma_2 \approx -0.74$ . We have also analyzed tendril solutions associated with the withdrawal flows generated by a ring vortex and by a point sink and found the same qualitative outcome. The differences in geometry between these withdrawal flows result in slightly different tendril shapes and values of  $\gamma_1$  and  $\gamma_2$ . Using (9), we have estimated how quickly two miscible layers will mix in thermal convection and found results consistent with observed values. However, the strong dependence on  $E$  of (9) makes a precise comparison difficult. To fully establish how the tendril persists over time, a complete numerical study as well as an experiment where the withdrawal is generated directly, e.g., by withdrawing liquid from a tube inserted into the upper layer [2,8,9], instead of indirectly via thermal convection, are needed.

Aside from providing an estimate for  $Q_0$  that takes into account the interior stagnation point, our analysis also reveals that, although some information about the large-scale flow is necessary to specify a tendril shape, the

dependence on the large-scale flow geometry is weak. This may explain why tendrils in thermal convection experiments can remain stable over long periods of time despite fluctuations in the global convection which can alter the large-scale topography.

The authors thank Anne Davaille, Sarah C. Case, Leo P. Kadanoff, and Sidney R. Nagel for encouragement and helpful discussions. This work was supported by the DOE (L. E. S.) and NSF No. CBET-0730629 (W. W. Z).

- [1] A. Davaille, *J. Fluid Mech.* **379**, 223 (1999); M. Le Bars and A. Davaille, *J. Fluid Mech.* **499**, 75 (2004).
- [2] S. Courrech du Pont and J. Eggers, *Phys. Rev. Lett.* **96**, 034501 (2006).
- [3] J. T. Jeong and H. K. Moffatt, *J. Fluid Mech.* **241**, 1 (1992).
- [4] S. Blake and G. N. Ivey, *J. Volcanol. Geotherm. Res.* **27**, 153 (1986); J. R. Lister, *J. Fluid Mech.* **198**, 231 (1989).
- [5] A. M. Gñan Calvo, M. Perez-Saborid, J. M. Lopez-Herrera, and J. M. Gordillo, *Eur. Phys. J. B* **39**, 131 (2004); R. Suryo and O. A. Basaran, *Phys. Fluids* **18**, 082102 (2006); S. L. Anna, N. Bontoux, and H. A. Stone, *Appl. Phys. Lett.* **82**, 364 (2003).
- [6] P. G. Simpkins and V. J. Kuck, *Nature (London)* **403**, 641 (2000); J. Eggers, *Phys. Rev. Lett.* **86**, 4290 (2001); E. Lorenceau, F. Restagno, and D. Quére, *Phys. Rev. Lett.* **90**, 184501 (2003); E. Lorenceau, D. Quére, and J. Eggers, *Phys. Rev. Lett.* **93**, 254501 (2004).
- [7] I. Cohen, H. Li, J. L. Houglund, M. Mrksich, and S. R. Nagel, *Science* **292**, 265 (2001); J. L. Wyman, S. Kizilel, R. Skarbek, X. Zhao, M. Connors, W. S. Dillmore, W. L. Murphy, M. Mrksich, and S. R. Nagel, *Small* **3**, 683 (2007).
- [8] S. C. Case and S. R. Nagel, *Phys. Rev. Lett.* **98**, 114501 (2007).
- [9] I. Cohen and S. R. Nagel, *Phys. Rev. Lett.* **88**, 074501 (2002).
- [10] W. W. Zhang, *Phys. Rev. Lett.* **93**, 184502 (2004).
- [11] A. M. Jellinek and M. Manga, *Nature (London)* **418**, 760 (2002).
- [12] A. Davaille, F. Girard, and M. Le Bars, *Earth Planet. Sci. Lett.* **203**, 621 (2002).
- [13] A. M. Jellinek and M. Manga, *Rev. Geophys.* **42**, RG3002 (2004).
- [14] N. H. Sleep, *Geophysical Journal* **95**, 437 (1988).
- [15] A. Davaille, Poster, Focusing Stress in a Soft Interface Workshop (U. Chicago, Chicago, 2005).
- [16] A. Acrivos and T. S. Lo, *J. Fluid Mech.* **86**, 641 (1978); G. I. Taylor in *Proceedings of the 11th International Congress on Applied Mechanics, Munich, Germany, 1964* (Springer, Heidelberg, 1966).
- [17] L. E. Schmidt and W. W. Zhang (unpublished).
- [18] S. H. Lee, R. S. Chadwick, and L. G. Leal, *J. Fluid Mech.* **93**, 705 (1979).
- [19] Here we have chosen the simpler option of matching  $R_I(z)$  and  $R(z)$  at a point instead of systematically matching them. Our numerics show the tendril merges smoothly onto  $R_I(z)$ , so the errors appear small. This choice also reveals the parameter dependencies explicitly.